RSC Advances

RSC Publishing

PAPER

View Article Online
View Journal | View Issue

Cite this: *RSC Advances*, 2013, **3**, 19366

Additive-free solvothermal synthesis of hierarchical flower-like $LiFePO_4$/C mesocrystal and its electrochemical performance

Nan Zhou,*[abc] Evan Uchaker,[b] Hai-Yan Wang,[c] Ming Zhang,[b] Su-Qin Liu,[c] You-Nian Liu,[c] Xiongwei Wu,[a] Guozhong Cao[b] and Huiyong Li*[a]

Received 8th June 2013,
Accepted 12th August 2013

DOI: 10.1039/c3ra42855a

www.rsc.org/advances

Three dimensional hierarchical flower-like lithium iron phosphate ($LiFePO_4$) mesocrystals were successfully synthesized *via* a solvothermal approach with the utilization of a mixture of water/ethylene glycol/dimethylacetamide (H_2O/EG/DMAC) as co-solvent. No other surfactant or template agent was used and beautiful micro-sized $LiFePO_4$ mesoporous structures with a special rose-like morphology were obtained. The hierarchical $LiFePO_4$ mesocrystals were assembled by well crystallized nano-sized $LiFePO_4$ thin plates with a thickness around 100 nm. The characteristics and electrochemical dynamics as well as performance of the obtained hierarchical flower-like $LiFePO_4$ mesocrystals were carefully investigated. The flower-like hierarchical $LiFePO_4$ mesocrystals showed a high initial lithium intercalation capability of 147 mA h g^{-1} at a current density of 17 mA g^{-1} (0.1 C), which should be attributed to the high specific surface area resulting from the mesoporous superstructure and well crystallized $LiFePO_4$ nano-plate composition units. Polyvinylpyrrolidone (PVP) was introduced during the solvothermal synthesis as an *in situ* carbon coating source. The obtained flower-like C-coated $LiFePO_4$ mesocrystals exhibited even better initial lithium intercalation capability of 161 mA h g^{-1} at 0.1 C and showed improved lithium storage performance at high rates as well as good cyclic stability.

1 Introduction

With the over developed modern society, the need for high power and high energy rechargeable lithium ion batteries (LIBs) has grown to a new level.[1,2] As one of the most promising cathode materials for new generation LIBs, olivine-base lithium iron phosphate ($LiFePO_4$ or in short LFP hereafter) has been of interest for its high theoretical capacity, low cost, long cycle life and superior safety and stability.[3] However, poor lithium ion and electronic conductivity was found in LFP due to the intrinsic crystal deficiency,[4–7] largely hindering its wide-spread commercialization.[8–10] The good combination of hierarchical three-dimensional mesoscopic structure with *in situ* carbon coating, which takes the advantages of high surface area and porosity, small size, well crystallized composition units, as well as easy process ability, is a good way to address the aforementioned problem and offers unique new opportunities for advanced $LiFePO_4$ material design.[11,12] A few micro-scale hierarchical $LiFePO_4$ assemblies with different shapes have been successfully synthesized, characterized and reported.[13–16] Recently, mesocrystals (mesoscopically structured crystals) have been attracting a lot of attention due to the different collective properties of their individual nanoparticles or bulk materials.[17] As a new class of solid material superstructures that are composed of a few to thousands of hierarchically assembled nano-scale primary units, mesocrystals also offer large surface area, high porosity, and small size primary units, which in combination make them perfectly suited for new LFP material design. Mesocrystals have already been fabricated and used for energy storage and conversion,[18,19] and the synthesis and fabrication of $LiFePO_4$ mesocrystals has been started recently. Fagot-like and sheaf-like $LiFePO_4$ mesocrystals were fabricated from $Fe_3(PO_4)_2(H_2O)_8$ precursors through a hydrothermal route by Uchiyama's group.[20] The influence of organic additive and precursor on the morphology of the LFP mesocrystals was carefully investigated. However, the electrochemical property of the obtained LFP mesocrystals was not determined. Urchin-like LFP mesocrystals were prepared through a template-free solvothermal route by Popovic *et al.*[21] After *in situ* carbon coating, the urchin-like $LiFePO_4$ mesocrystals exhibited a 100 mA h g^{-1} lithium intercalation capacity at 0.1 C rate. Unfortunately, expensive organic surfactants were employed

[a]*College of Science, Hunan Agricultural University, Changsha, Hunan, 410128, China. E-mail: lhy5321@hunau.net; Fax: 86-731-8461 8071; Tel: 86-731-8467 3585*
[b]*Department of Materials Science and Engineering, University of Washington, Seattle, Washington, 98195, United States. E-mail: nan_zhou@outlook.com; Fax: 86-731-8461 8071; Tel: 86-731-8467 3585*
[c]*College of Chemistry and Chemical Engineering, Central South University, Changsha, Hunan, 410083, China*

in most of those aforementioned works, and complicated processes as well as long reaction times were needed. Besides, investigations into the electrochemical dynamics of $LiFePO_4$ mesocrystals are still lacking.

Among all the synthetic approaches, solvothermal synthesis is considered to be one of the most efficient ways to have phase purity, grain size and particle morphology controlled, where various solvents and surfactants are largely applied.[22,23] Recently, we reported the additive-free solvothermal synthesis of hierarchical dumbbell-shaped $LiFePO_4$ mesocrystals by using dimethylformamide/ethylene glycol (DMF/EG) as co-solvent.[24] Although the exact mechanism remains unclear, the amide plays a crucial way in the formation of hierarchical dumbbell-like LFP mesocrystals and the products can only be obtained within EG/DMF co-solvent. High lithium-ion intercalation capacity was obtained for this $LiFePO_4$ mesocrystal due to the fast intercalation reaction and easy mass and charge transfer offered by the large specific surface and short diffusion distance of dumbbell-shaped mesoporous structures composed of nanosized $LiFePO_4$ rods. In this work, another new amide of dimethylacetamide (DMAC) was employed as part of the co-solvent and three-dimensional hierarchical flower-like $LiFePO_4$ mesocrystals were synthesized *via* solvothermal route by using H_2O/EG/DMAC co-solvent without any surfactant or additive. The characterization, formation mechanism and electrochemical dynamics as well as performance of this hierarchical superstructure were carefully investigated. The mesocrystals can be *in situ* carbon coated by introducing PVP during the solvothermal synthesis and the PVP has no effect on the formation of the LFP mesocrystals. The hierarchical flower-like $LiFePO_4$-carbon mesocrystals exhibited improved electrochemical property and good cyclic stability.

2 Experimental

2.1 Synthesis

Three-dimensional hierarchical flower-like $LiFePO_4$ mesocrystals were synthesized *via* solvothermal route by using lithium dihydrogen phosphate LiH_2PO_4($\geqslant$99.0%, Aesar) and Ferrous sulfate heptahydrate $FeSO_4{\cdot}7H_2O$($\geqslant$99.0%, Aldrich) as precursors. 10.0 mmol $FeSO_4{\cdot}7H_2O$ was first dissolved in 4.45 ml EG while a stoichiometric amount of LiH_2PO_4 was dissolved in 4.45 ml DMAC/1.1 ml H_2O co-solvent separately. Then the two solutions were mixed together and ultrasonicated for 10 min. The overall molar ratio of Li : Fe : P was 1 : 1 : 1. The obtained mixture was transferred into a 30 ml PTFE inner steel autoclave and heated at 225 °C for 4 h. After that, the autoclave was taken out of the furnace and fast cooled to room temperature. The obtained product was washed with ethanol and de-ionized water several times. For carbon coated flower-like $LiFePO_4$/C mesocrystals, 1.5 g PVP was added with LiH_2PO_4 in the DMAC/H_2O co-solvent before the mix and ultrasonic treatment. The carbon content of the flower-like LFP/C mesocrystals was calculated according to the TGA results, and it turned out to be about 4.2 wt%. The obtained pure and carbon coated $LiFePO_4$ mesocrystals were dried at 60 °C overnight followed by annealing in nitrogen gas environment for a dwell time of 5 h at 600 °C to guarantee better crystallinity and conductive coating. No other surfactants or template agents were added during the solvothermal synthesis.

To study the formation mechanism of the hierarchical flower-like $LiFePO_4$ mesocrystals, solvothermal syntheses were carried out with different duration times of 1, 2 and 3 h, with other conditions unchanged. For convenience, sample notations are used in this paper: the products obtained from various reaction times of 1, 2 and 3 h are noted as S_{1h}, S_{2h}, and S_{3h} respectively. The LFP mesocrystals without further calcinations were also analyzed by XRD and SEM to determine the crystal phase and product morphology after 4 h solvothermal reaction.

2.2 Structural characterization

Scanning electron microscopy (SEM) was performed with a JEOL JSM-7000F field emission scanning electron microscope. X-Ray Diffraction (XRD) was carried out in a D8 Bruker X-ray diffractometer under a scan speed of $0.02^\circ\ s^{-1}$ in the 2θ range from 10 to 60°. High-resolution transmission electron microscopy (HRTEM) images were taken by a Tecnai G2 F20 transmission electron microscope. Raman spectra were performed to study the structure of the pure and carbon coated $LiFePO_4$ mesocrystals by using a LabRAM ARAMIS spectrometer (Horiba Jobin Yvon, France). Thermogravimetric analysis (TGA) (PerkinElmer instruments) was utilized to calculate the carbon content of the flower-like $LiFePO_4$/C mesocrystals. Brunauer–Emmett–teller (BET) was utilized to examine the surface areas of samples.

2.3 Property measurements

The obtained samples were mixed with super P carbon black and poly(vinyl difluoride) (PVDF) in the weight ratio 75 : 15 : 10 using *N*-methyl pyrrolidone (NMP) as solvent and then pasted on an aluminum foil to fabricate composite electrodes and then assembled into R2016 coin-type cells in an argon filled glove box. Lithium metal foil, 1 M $LiPF_6$ in ethylene carbonate (EC)/dimethyl carbonate (DMC) (1 : 1, in weight) and Celgard 2502 membrane were used as counter electrode, electrolyte and separator, respectively. Cyclic voltammetry (CV) was performed under different scanning rates on a CHI660B electrochemical workstation (shanghai, China) at ambient temperature. Electrochemical impedance spectroscopy (EIS) measurements were performed with an excitation signal of 5 mV in an alternating current frequency range of 0.01 to 100 kHz using a Princeton electrochemical workstation (Parstat 2273). The galvanostatic charge-discharge tests at constant current mode were carried out using a computer controlled electrochemical analyzer (Land, China) in the voltage range of 4.2–2.5 V (*vs.* Li/Li^+).

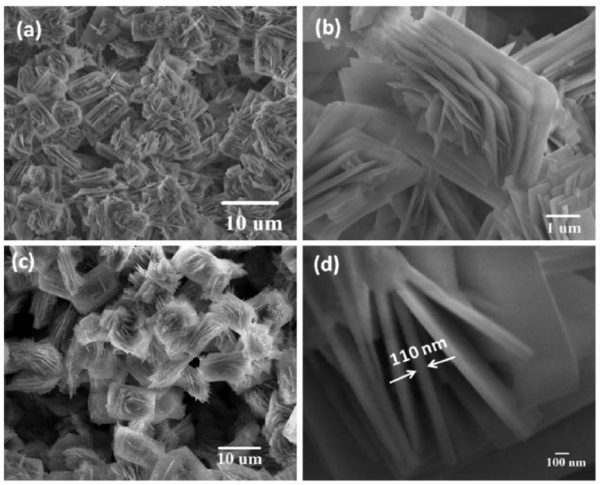

Fig. 1 SEM images of pure (a, b) and carbon coated (c, d) hierarchical flower-like $LiFePO_4$ mesocrystals.

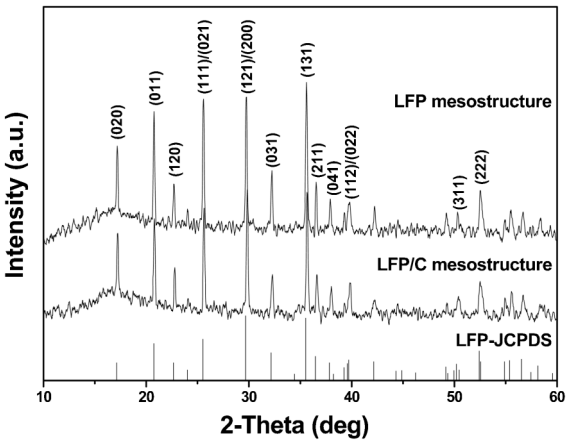

Fig. 2 XRD pattern of pure and carbon coated hierarchical flower-like $LiFePO_4$ mesocrystals.

3 Results and discussion

3.1 Structure characterization

Fig. 1 shows the SEM images of the hierarchically pure (Fig. 1 (a) (b)) and carbon coated (Fig. 1 (c) (d)) $LiFePO_4$ mesocrystals at various magnifications. Three-dimensional hierarchical flower-like $LiFePO_4$ mesocrystals with a size of around 10 μm were fabricated through solvothermal route by using the H_2O/EG/DMAC co-solvent, without any additive or surfactant. This unique mesocrystal flower has beautiful oblong petals and seems like two roses grown on both sides of a big rectangle $LiFePO_4$ nano-plate with a size about 8 × 10 μm. After *in situ* carbon coating, the $LiFePO_4$/C mesocrystals with the same hierarchical flower-like shape were obtained, suggesting that the introduction of carbon has no effect on the morphology of the hierarchical flower-like mesostructures. SEM image with higher magnification (Fig. 1 (d)) shows that the primary units of the carbon coated LFP mesocrystals are nano-sized LFP plates with a thickness about 110 nm. Those $LiFePO_4$ nano-plates were grown branched with each other rather than organized aggregation arrays. Thus, the obtained pure and carbon coated flower-like $LiFePO_4$ mesocrystals are all holding a highly porous structure, leading to high BET surface areas of 24.9 and 15.1 $m^2\ g^{-1}$ for LFP and LFP/C mesocrystals, respectively.

Fig. 2 shows the XRD patterns of the pure and carbon coated hierarchical flower-like $LiFePO_4$ mesocrystals obtained from solvothermal synthesis followed with further annealing at 600 °C for 5 h. Also included in Fig. 2 is the standard XRD pattern for $LiFePO_4$ material. Both XRD patterns of the pure and C-coated samples are indexed to a well crystallized orthorhombic olivine $LiFePO_4$ material (JCPDS card #040-1499), without any secondary phases such as FeP, $FePO_4$ or Li_3PO_4. The lattice parameters of these two $LiFePO_4$ mesocrystals are calculated from the XRD results: 1) *a* - 10.3316 Å, *b* - 6.0058 Å, *c* - 4.6996 Å for the LFP mesocrystals; and 2) *a* - 10.3279 Å, *b* - 5.9997 Å, *c* - 4.6935 Å for the LFP/C mesocrystals, respectively, all of which agree well with those values reported in literature.[25] Thus, it can be concluded that: 1) pure $LiFePO_4$ materials can be synthesized during this simple solvothermal route by using H_2O/EG/DMAC co-solvent followed with calcinations at 600 °C for 5 h, even though short reaction time of 4 h and no additive or surfactant was applied; 2) carbon pyrolyzed from PVP is likely to be amorphous and has no impact on the morphology and crystallinity of the $LiFePO_4$ material.

Fig. 3 shows the TEM and HRTEM images of the carbon free and coated hierarchical flower-like $LiFePO_4$ mesocrystals.

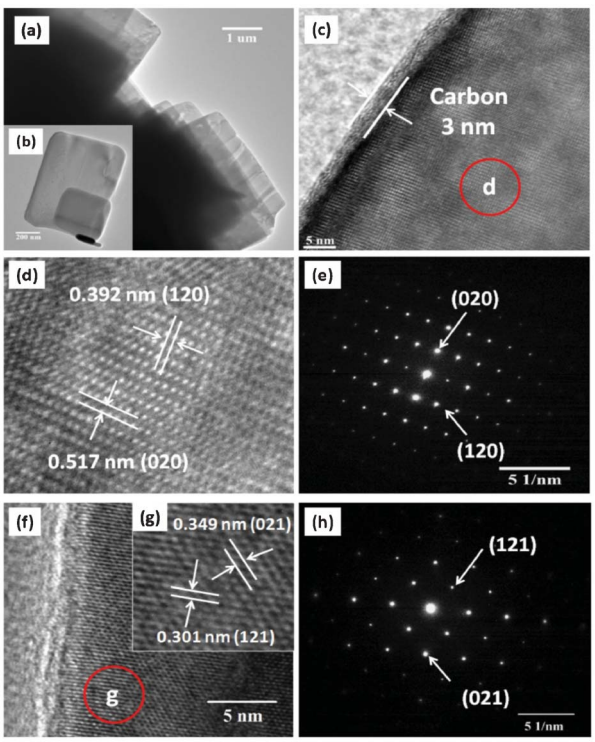

Fig. 3 HRTEM images and SAED patterns of carbon coated (a)–(e) and carbon free (f)–(h) hierarchical flower-like $LiFePO_4$ mesocrystals.

Fig. 3 (a) and (b) (inset) reveal that the composition units of the carbon coated hierarchical flower-like $LiFePO_4$ mesocrystals are oblong LFP plates with different sizes, which corroborates well with the SEM images. Fig. 3 (c) and (f) are the HRTEM images of the edge part of the rectangular LFP nano-plate with and without nanocarbon coating. The neat lighter layer around the architecture in Fig. 3 (c) depicts the homogeneous carbon coating layer that results from PVP pyrolysis, while no such layer is apparent in the carbon-free LFP mesocrystals in Fig. 3 (f). The average thickness of the carbon layer is approximately 3 nm and the carbon content calculated from TGA result is about 4.2 wt%. The lattice fringes of the carbon coated LFP mesocrystals enlarged in HRTEM image Fig. 3 (d) have d-spacing values of 0.517 and 0.392 nm, corresponding to the (020) and (120) planes of the orthorhombic phase $LiFePO_4$. While the HRTEM image Fig. 3 (g) (insert) shows the lattice fringes of the pure LFP mesocrystals with d-spacing values of 0.349 and 0.301 nm, corresponding to the (021) and (121) planes of the orthorhombic phase $LiFePO_4$. All of which confirms that $LiFePO_4$ mesocrystals can be obtained during the solvothermal synthesis in the co-solvent of H_2O/EG/DMAC, with or without *in situ* carbon sources. Besides, single crystalline patterns with sharp diffraction dots were obtained for the selected area electron diffraction (SAED) analysis (Fig. 3 (e) and (h)) of both samples, further confirming that the primary units of the flower-like $LiFePO_4$ mesocrystals are well crystallized olivine LFP material and *in situ* carbon coating has no effect on the crystal phase of $LiFePO_4$ materials.

Raman spectra were performed to study the surface structure of the hierarchical flower-like LFP and LFP/C mesocrystals, and the results are shown in Fig. 4. Both Raman spectra of the two mesocrystals show intensive peaks attributed to the orthorhombic $LiFePO_4$ with intramolecular stretching vibration of PO_4^{3-} anions recorded at 586, 990 and 1040 cm^{-1}, further confirming the good crystallization of LFP composition units in the mesocrystals. Different from the smooth curve of flower-like LFP mesocrystals, small peaks appeared at 1380 and 1550 cm^{-1} in the spectrum of flower-like

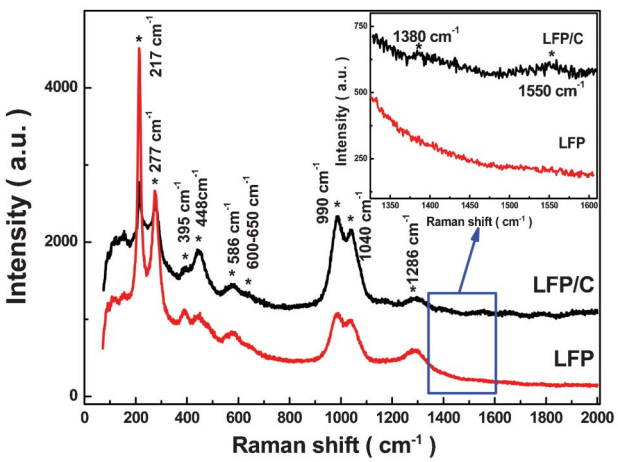

Fig. 4 Raman spectra of pure and carbon coated hierarchical flower-like $LiFePO_4$ mesocrystals.

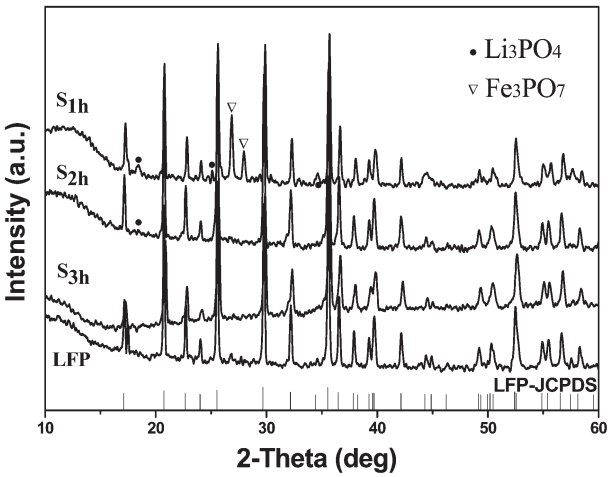

Fig. 5 XRD patterns of samples derived from different reaction times.

LFP/C mesocrystals, which correspond to the carbon-based contamination vibration, indicating the small amount of conductive carbon coating residue from PVP pyrolysis.

3.2 Formation mechanism

Time-dependent solvothermal synthesis experiments were carefully carried out to study the formation mechanism of the flower-like $LiFePO_4$ mesocrystals, with other parameters remaining unchanged. The obtained products as well as the pure flower-like $LiFePO_4$ mesocrystals without the high temperature calcination treatment were carefully investigated by XRD and SEM analysis, and the results are shown in Fig. 5 and 6. The XRD pattern of the product obtained from 1 h reaction already shows intensive peaks corresponding to the orthorhombic $LiFePO_4$, indicating the reaction has already proceeded to the formation of $LiFePO_4$ materials even though such a short reaction time was applied. Two small peaks indexed to Li_3PO_4 were detected in this sample, which should be attributed to the nuclei growth precursor since phase transformation from Li_3PO_4 crystal to $LiFePO_4$ crystal was likely to happen, which is widely reported in the literature.[13,26] Fe^{3+} containing chemical Fe_3PO_7 was also detected in sample S_{1h}, possibly formed during the cooling process, indicating the formation of Li_3PO_4 crystals was not finished within 1 h. For sample S_{2h}, just one tiny peak corresponding to Li_3PO_4 remained and the Fe_3PO_7 phase disappeared, suggesting the formation of $LiFePO_4$ material was about to close, which was confirmed by the XRD pattern of sample S_{3h}, where intensive peaks corresponding to LFP were only detected without any other impurities. After 4 h reaction, diffraction peaks indexed to well crystallized $LiFePO_4$ with higher intensities were found in the XRD pattern of flower-like LFP mesocrystals, indicating the crystallinity of the LFP material increased with the extension of reaction time.

Fig. 6 shows the SEM images of the samples obtained from various solvothermal reaction durations as well as the pure flower-like LFP mesocrystals without calcinations. Nanoscaled particles or spheres with a few oblong nano-plates were found in the sample obtained from 1 h reaction, as shown in Fig. 6

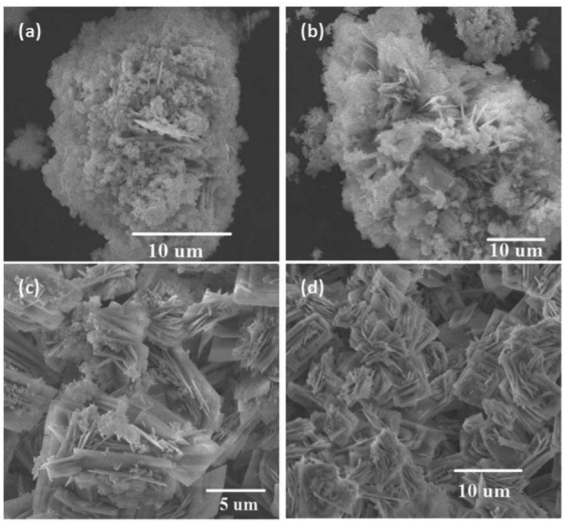

Fig. 6 SEM images of samples (a) S_{1h}, (b) S_{2h}, (c) S_{3h} and pure flower-like $LiFePO_4$ mesocrystals without annealing treatment.

(a), indicating the formation of $LiFePO_4$ nano-plates has already started even in such a short reaction time. More nano-platelet products and fewer spheres were detected when the solvothermal duration was extended to 2 h (Fig. 6 (b)), confirming the gradual growth of the $LiFePO_4$ nano-plates from the precursor particles. For the first two samples, most of the products were aggregated together. This is a common case in most of the nanostructure materials,[27–29] but the agglomeration of the products makes it very difficult to detect the initial formation of the flower-like $LiFePO_4$ mesocrystals. Many flower-like LFP mesocrystals appeared in the sample S_{3h} (Fig. 6 (c)), however, the structure sizes of those mesocrystals were smaller than the pure flower-like LFP mesocrystals obtained after 4 h reaction (Fig. 6 (d)). Besides, a few particles and plates could still be found in sample S_{3h}, indicating the assembly of the LFP mesocrystals was not finished within 3 h.

Fig. 7 schematically summarizes the formation mechanism of the flower-like $LiFePO_4$ mesocrystals, which was likely a two step process. First, nucleation growth of Li_3PO_4 crystals and the formation of LFP nano-plates from precursor particles; and then phase transformation from Li_3PO_4 to $LiFePO_4$ crystals combined with nano-plate self-assembly to LFP mesocrystals. Some authors attributed the formation of LFP mesostructures to van der Waals attraction[26] or lattice tension and surface interaction[13] resulting from the utilization of organic surfactant or template agent. However, our work revealed that no surfactant or additive was necessary with the application of H_2O/EG/DMAC co-solvent, by which interface energy, chemistry or ion diffusivity might be provided. It seems that the existence of the co-solvent played an important role in the formation of the flower-like $LiFePO_4$ mesocrystals. However, the influence of the co-solvent on the formation mechanism was not studied in this work, since the application of three different solvents makes the reaction a very complicated process and requires further and deeper investigations.

3.3 Electrochemical dynamics and performance

The hierarchical flower-like $LiFePO_4$ and carbon coated mesocrystals were mixed with carbon black and binder to fabricate cathode films and then assembled into R2016 coin-type cells in an Argon-filled glove box respectively. To investigate the intrinsic kinetics of the lithium ion in the hierarchical flower-like $LiFePO_4$ and $LiFePO_4$/C mesocrystals, cyclic voltammetric (CV) analysis was carefully performed under various scanning rates. Fig. 8 shows the CV curves (Fig. 8 (a) (b)) of these two $LiFePO_4$ mesocrystal cathodes at different scanning rates range from 0.05 to 1 mV S^{-1} and the fitting lines (Fig. 8 (c) (d)) obtained from the CV results. Only one couple of cathodic and anodic peaks was found in the range of 3.1–3.8 V (*vs.* Li/Li^+) for both samples with different scanning rates. These well defined redox peaks represent the transformation of Fe^{2+}/Fe^{3+} phases, which corresponds to the intercalation/deintercalation of lithium ions from $LiFePO_4$ crystals. For each CV curve of both pure and C-coated LFP mesocrystals, similar peak shapes and areas were detected for the corresponding cathodic and anodic peaks, indicating the good reversibility of the lithium ion intercalation/deintercalation for both samples. In addition, the cathodic and anodic peaks move to lower and higher potentials respectively with the increase of scanning rate, combined with larger peak areas and higher magnitude of peak currents (I_p). Sharper peaks and lower valued hysteresis (ΔV = the difference between the anodic and cathodic peak voltages) were found for carbon coated hierarchical flower-like $LiFePO_4$ mesocrystals when compared with carbon free ones. It is reported that there is a narrow gap between the redox peaks indicating more effective

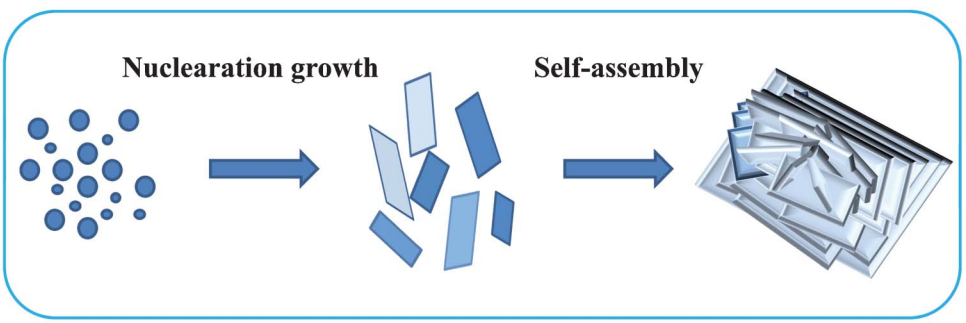

Fig. 7 Schematic illustration of the formation of hierarchical flower-like $LiFePO_4$ mesocrystals.

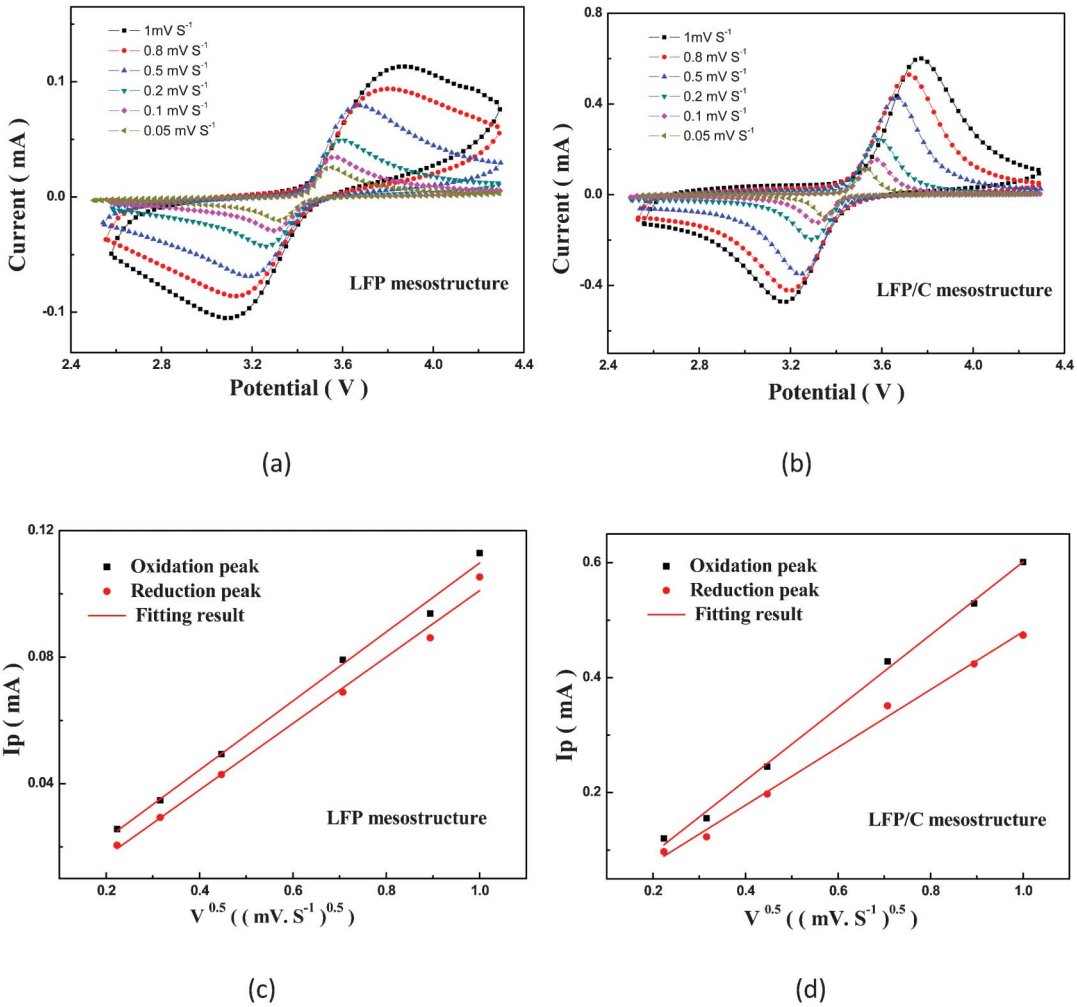

Fig. 8 CV curves and fitting lines of pure (a, c) and carbon coated (b, d) hierarchical flower-like $LiFePO_4$ mesocrystals.

redox reactions,[30] thus, faster transition of lithium ions and phase transformation should be found in carbon coated $LiFePO_4$ mesocrystals, which should facilitate better lithium intercalation/deintercalation properties.

For semi-infinite and finite diffusion systems, the peak current (I_p) would be proportional to the square root of the scan rate (v),[31] according to which the diffusion coefficient can be calculated based on the Randles–Sevcik equation:[32]

$$I_p = 2.69 \times 10^5 ACD^{1/2} n^{3/2} v^{1/2} \quad (1)$$

where A is the dipped area of the electrode into the electrolyte solution, for the composite LFP or LFP/C electrodes, A should be the real reaction area of the active materials. Thus, the BET surface area was taken as the effective area A for both samples. n is the number of electrons involved in the redox process (for Fe^{2+}/Fe^{3+} it is 1), v is the potential scan rate (V s^{-1}), D is the diffusion coefficient of Li in the electrode (cm^2 s^{-1}), C is the Li concentration, for $LiFePO_4$ material with a bulk density of 3.6 g cm^{-3} and a molar mass of 157.76 g mol^{-1}, for which the corresponding Li concentration C should be 0.0228 mol cm^{-3}.

Two fitting lines based on the magnitudes of the cathodic and anodic peak currents I_p and the square root of the scanning rate v can be obtained for each sample (Fig. 8 (c) (d)), according to which the diffusion coefficient D can be calculated. The Li ion diffusion coefficient of the pure hierarchical flower-like $LiFePO_4$ mesocrystals were 1.19×10^{-14} and 1.31×10^{-14} cm^2 s^{-1} for the anodic and cathodic reactions respectively, and the Li ion diffusion coefficient of the carbon coated hierarchical flower-like $LiFePO_4$ mesocrystals were 1.30×10^{-12} and 0.82×10^{-12} cm^2 s^{-1} respectively, as summarized in Table 1. The order of the anodic and cathodic diffusion coefficient remains the same for both LFP mesocrystals, indicating the excellent reversibility of the lithium intercalation/deintercalation processes. The carbon coated flower-like $LiFePO_4$ mesocrystal has two orders higher lithium diffusion coefficients than its pure counterpart, confirming the faster redox reaction and better electrochemical performance of this sample, which should be attributed to the homogeneously coated nanocarbon.

To analyze the inner impedance of the pure and carbon coated flower-like LFP mesocrystal electrodes, EIS tests of these two samples were carried out at open circuit under

Table 1 Linear fitting results of the relationship of I_p-$v^{1/2}$

Sample		k/(As$^{0.5}$ V$^{-0.5}$)	R	D/cm^2 s^{-1}
LFP mesocrystal	Anodic peak	0.109	0.9934	1.19×10^{-14}
	Cathodic peak	0.105	0.9920	1.31×10^{-14}
LFP/C mesocrystal	Anodic peak	0.634	0.9969	1.30×10^{-12}
	Cathodic peak	0.503	0.9938	0.82×10^{-12}

ambient temperature. Before EIS tests, all the cells were subjected to charge and discharge for 3 cycles to activate the layer formation and guarantee the electrolyte penetration. The obtained Nyquist plots of pure and C-coated LFP mesocrystals are shown in Fig. 9. For both samples, a semicircle in the high frequency region and a sloping line in the low frequency region were found. The semicircle at high frequency should correspond to the impedance of the contact between particle-to-particle and particle-to-current collector or the impedance of the passivating layer,[33–36] while the sloping line at low frequency should be attributed to the diffusion of the Li ion inside the host materials.[37] To better understand the difference between the impedance kinetics of the pure and carbon coated flower-like LFP mesocrystals, an equivalent circuit (inset of Fig. 9) was employed to explain the obtained EIS spectra. The resistor R_s corresponds to the resistance of the electrolyte, R_{ct} represents the resistance of charge transfer, CPE is the constant phase element related to R_{ct}, and Z_w is the Warburg impedance describes the diffusion of Li ions inside the active materials. Based on the diameter of the semicircles, the value of charge transfer resistance R_{ct} of pure and C-coated $LiFePO_4$ mesocrystals can be obtained, which were 456 and 261 Ω, respectively. Much smaller charge transfer resistance was found for the LFP/C mesocrystals, indicating faster charge transfer between the electrolyte and the LFP material in this sample. It can be concluded that the ionic conductivity of the flower-like LFP mesocrystals could be greatly enhanced by a homogeneously coated carbon layer, which corroborates well with the profiles of both CV and charge–discharge analysis.

Fig. 10 show the initial charge/discharge curves of pure and carbon coated hierarchical flower-like $LiFePO_4$ mesocrystals at a current density of 17 mA g^{-1} (0.1 C) in the voltage range of 2.5 to 4.2 V (*vs.* Li/Li$^+$). Since the capacity of carbon could be negligible in this voltage range, the mass of coated carbon was not included when calculating the specific capacity of the LFP/C composite electrodes. The pure hierarchical flower-like $LiFePO_4$ mesocrystals exhibited an initial charge capacity of about 167.7 mA h g^{-1} and an initial discharge capacity of about 147.1 mA h g^{-1}, very close to the theoretical value (170 mA h g^{-1}) of the LFP material. The high lithium storage performance should be attributed to the high porous structure of the LFP mesocrystals, which introduced large surface area to enlarge the interface between the electrolyte and the active materials. Combined with the well crystallized primary units of $LiFePO_4$ plates with nano-sized thickness, the hierarchical flower-like $LiFePO_4$ mesocrystals with large surface area and high porosity can greatly short the diffusion path of the lithium ions and accelerate the charge and mass transfer. After carbon coating, the hierarchical flower-like $LiFePO_4$/C mesocrystals showed an initial charge capacity of 159.3 mA h g^{-1} with a even higher initial discharge capability of 161.4 mA h g^{-1} at the same rate of 0.1 C, almost the theoretical value of LFP materials, confirming the conductivity of the $LiFePO_4$ mesocrystals can be effectively improved by *in situ* carbon coating. In addition, the gap between the charge and discharge curves of the C-coated LFP mesocrystals is much smaller than the one of the pure LFP mesocrystals, indicating faster redox reaction and phase transition of LFP mesocrystals with

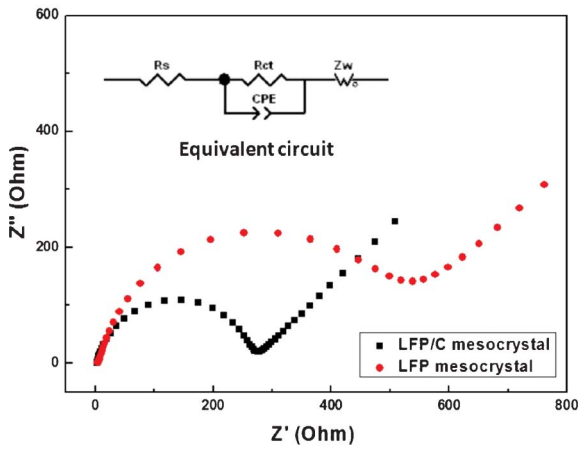

Fig. 9 Nyquist plots of LFP and LFP/C mesocrystals. Inset is the equivalent circuit.

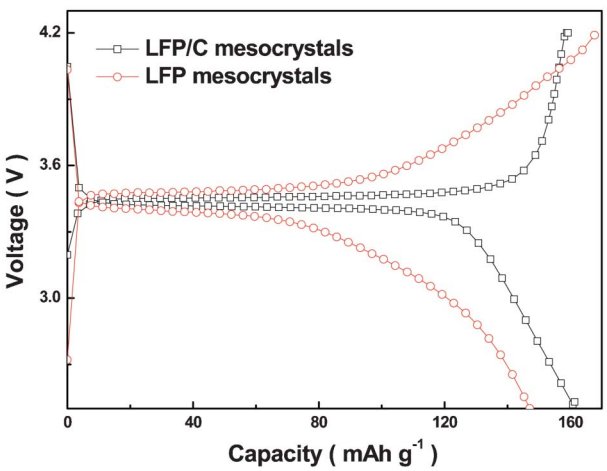

Fig. 10 Initial charge/discharge curves of pure and carbon coated hierarchical flower-like $LiFePO_4$ mesocrystals.

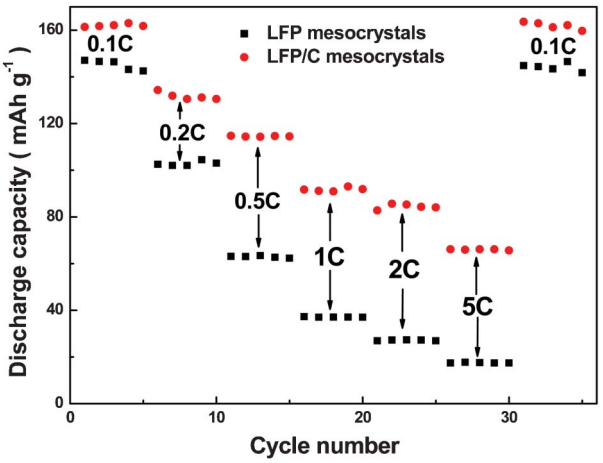

Fig. 11 Rate performance of pure and carbon coated hierarchical flower-like $LiFePO_4$ mesocrystals.

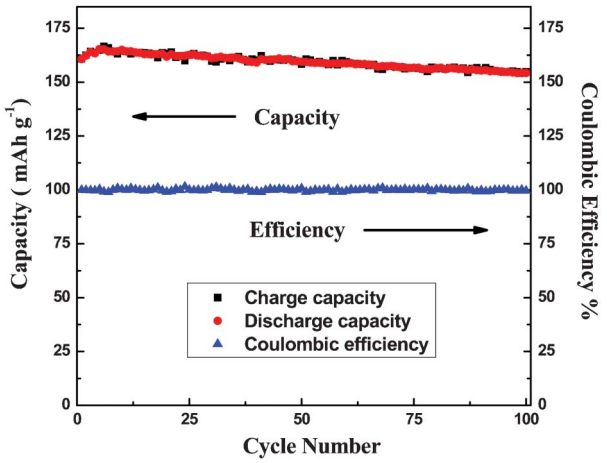

Fig. 12 Cyclic performance and Coulombic efficiency of the LFP/C mesocrystals at 0.1 C rate between 2.5–4.2 V.

nanocarbon coating. However, larger Li^+ intercalation property than deintercalation property was found for the initial cycle of C-coated flower-like LFP mesocrystals, suggesting the initial deficient amount of Li-ions in the C-coated mesocrystals, which might result from the addition of PVP combined with a short reaction duration of 4 h through solvothermal synthesis.

The rate capabilities of both pure and C-coated flower-like LFP mesocrystals were analyzed under different current densities for every 5 cycles, and the results are shown in Fig. 11. After 5 cycles at 0.1 C rate, the current density was increased stepwise to 5 C rate. With the increase of the current densities, the discharge capacities of both samples gradually decreased, which is a commonly case for electrodes. The LFP mesocrystals exhibited lower lithium ion storage capabilities of 102, 63, 37 and 27 mA h g^{-1} under different rates of 0.2, 0.5, 1 and 2 C, respectively, while much higher lithium intercalation capacities of 134, 114, 91 and 85 mA h g^{-1} were detected for the LFP/C mesocrystals under the same test conditions. Poor initial discharge capacity of 17 mA h g^{-1} was detected in the pure flower-like LFP mesocrystal electrode under high current density of 850 mA g^{-1} (5 C), while a 66 mA h g^{-1} capability was still obtained for its carbon coated counterpart. The hierarchical flower-like $LiFePO_4$ mesocrystals show greatly improved electrochemical properties after *in situ* carbon coating, which should be attributed to the faster lithium ion diffusion and electron transfer brought by the homogeneously coated conductive carbon layer.

Fig. 12 is the cycling performance of the carbon coated hierarchical flower-like $LiFePO_4$ mesocrystals under 0.1 C rate; also included in Fig. 12 is the Coulombic efficiency (calculated from discharge capacity/charge capacity). The C-coated LFP mesocrystals showed an initial discharge capacity of about 160 mA h g^{-1} and then the capacity gradually increased at the first few cycles. The increase of the capacity during the first few cycles should possibly result from the gradual penetration of the electrolyte into the interior of the electrode materials and the progressive formation of the active surface layer; besides, cracks in the amorphous carbon coating layer might also be formed stepwise—all of which contribute to the gradually improved capacities. A similar phenomenon has been reported and discussed in the literature[38–40] and commonly happens in many carbon coated materials.[41] The charge and discharge capacity of the carbon coated hierarchical flower-like $LiFePO_4$ mesocrystals became steady after 6 cycles and then remained at around 160 mA h g^{-1} for dozens of cycles. Only 4% of the discharge capacity was lost after 100 cycles under the current density of 17 mA g^{-1} (0.1 C) for this electrode. The good cyclic stability of this mesocrystal should be attributed to the homogeneously coated nanocarbon. Besides, the Coulombic efficiency of the flower-like LFP/C mesocrystals maintained above 99% for all the charge and discharge processes, confirming the excellent reversibility of this sample, which agrees well with the CV results.

4 Conclusions

Hierarchical flower-like $LiFePO_4$ mesocrystals were successfully synthesized *via* a one-step, simple, additive-free solvothermal route. Three solvents of water, EG and DMAC were mixed together and applied to the solvothermal synthesis. Hierarchical micro-sized $LiFePO_4$ mesoporous structures with a special rose-like morphology were obtained and the composition units of the flower-like LFP mesocrystals were well crystallized nano-sized $LiFePO_4$ thin plates with a thickness of about 100 nm. Both the pure and carbon coated $LiFePO_4$ mesocrystals were annealed at 600 °C for 5 h to increase the crystallinity. High initial lithium intercalation capacities of 147 and 161 mA h g^{-1} were exhibited by pure and carbon coated $LiFePO_4$ mesocrystal at 0.1 C rate, respectively. The good electrochemical performances of both LFP mesocrystals should be attributed to the fast intercalation reaction and easy charge transfer facilitated by the large specific surface area of the flower-like mesoporous structure. The flower-like $LiFePO_4$ mesocrystals can be *in situ* carbon coated by adding PVP during the solvothermal process and the

electrochemical performance of the C-coated sample was effectively enhanced after homogeneous carbon coating.

Acknowledgements

NZ gratefully acknowledges a fellowship from the China Scholarship Council. This research work has been financially supported in part by the National Science Foundation (NSF, CMMI-1030048) and the University of Washington TGIF grant.

References

1 M. Armand and J. M. Tarascon, *Nature*, 2008, **451**, 652–657.
2 J. Yan, A. Sumboja, E. Khoo and P. S. Lee, *Adv. Mater.*, 2011, **23**, 746–750.
3 A. S. Andersson, J. O. Thomas, B. Kalska and L. Haggstrom, *Electrochem. Solid-State Lett.*, 2000, **3**, 66–68.
4 C. Wang and J. Hong, *Electrochem. Solid-State Lett.*, 2007, **10**, A65–A69.
5 K. Zaghib, A. Mauger, J. B. Goodenough, F. Gendron and C. M. Julien, *Chem. Mater.*, 2007, **19**, 3740–3747.
6 M. S. Islam, D. J. Driscoll, C. A. J. Fisher and P. R. Slater, *Chem. Mater.*, 2005, **17**, 5085–5092.
7 A. S. Andersson, B. Kalska, L. Haggstrom and J. O. Thomas, *Solid State Ionics*, 2000, **130**, 41–52.
8 C. Delacourt, L. Laffont, R. Bouchet, C. Wurm, J. B. Leriche, M. Morcrette, J. M. Tarascon and C. Masquelier, *J. Electrochem. Soc.*, 2005, **152**, A913–A921.
9 W. Ojczyk, J. Marzec, K. Świerczek, W. Zając, M. Molenda, R. Dziembaj and J. Molenda, *J. Power Sources*, 2007, **173**, 700–706.
10 D. Morgan, A. Van der Ven and G. Ceder, *Electrochem. Solid-State Lett.*, 2004, **7**, A30–A32.
11 V. Etacheri, R. Marom, R. Elazari, G. Salitra and D. Aurbach, *Energy Environ. Sci.*, 2011, **4**, 3243–3262.
12 J. Wang and X. Sun, *Energy Environ. Sci.*, 2012, **5**, 5163–5185.
13 H. Yang, X. L. Wu, M. H. Cao and Y. G. Guo, *J. Phys. Chem. C*, 2009, **113**, 3345–3351.
14 J. Qian, M. Zhou, Y. Cao, X. Ai and H. Yang, *J. Phys. Chem. C*, 2010, **114**, 3477–3482.
15 D. Rangappa, K. Sone, T. Kudo and I. Honma, *J. Power Sources*, 2010, **195**, 6167–6171.
16 Y. Xia, W. Zhang, H. Huang, Y. Gan, J. Tian and X. Tao, *J. Power Sources*, 2011, **196**, 5651–5658.
17 H. Colfen and M. Antonietti, *Angew. Chem., Int. Ed.*, 2005, **44**, 5576–5591.
18 L. Zhou and P. O'Brien, *Small*, 2008, **4**, 1566–1574.
19 R.-Q. Song and H. Coelfen, *Adv. Mater.*, 2010, **22**, 1301–1330.
20 H. Uchiyama and H. Imai, *Cryst. Growth Des.*, 2010, **10**, 1777–1781.
21 J. Popovic, R. Demir-Cakan, J. Tornow, M. Morcrette, D. S. Su, R. Schloegl, M. Antonietti and M.-M. Titirici, *Small*, 2011, **7**, 1127–1135.
22 S. Yang, X. Zhou, J. Zhang and Z. Liu, *J. Mater. Chem.*, 2010, **20**, 8086–8091.
23 K. Saravanan, P. Balaya, M. V. Reddy, B. V. R. Chowdari and J. J. Vittal, *Energy Environ. Sci.*, 2010, **3**, 457–464.
24 N. Zhou, H.-Y. Wang, E. Uchaker, M. Zhang, S.-Q. Liu, Y.-N. Liu and G. Cao, *J. Power Sources*, 2013, **239**, 103–110.
25 S. T. Myung, S. Komaba, N. Hirosaki, H. Yashiro and N. Kumagai, *Electrochim. Acta*, 2004, **49**, 4213–4222.
26 F. Teng, S. Santhanagopalan, A. Asthana, X. Geng, S.-i. Mho, R. Shahbazian-Yassar and D. D. Meng, *J. Cryst. Growth*, 2010, **312**, 3493–3502.
27 T. P. Chou, Q. Zhang, G. E. Fryxell and G. Cao, *Adv. Mater.*, 2007, **19**, 2588–2592.
28 Q. Zhang and G. Cao, *J. Mater. Chem.*, 2011, **21**, 6769–6774.
29 M. M. Khin, A. S. Nair, V. J. Babu, R. Murugan and S. Ramakrishna, *Energy Environ. Sci.*, 2012, **5**, 8075–8109.
30 J.-K. Kim, J.-W. Choi, G. S. Chauhan, J.-H. Ahn, G.-C. Hwang, J.-B. Choi and H.-J. Ahn, *Electrochim. Acta*, 2008, **53**, 8258–8264.
31 S. R. Das, S. B. Majumder and R. S. Katiyar, *J. Power Sources*, 2005, **139**, 261–268.
32 Y.-D. Cho, G. T.-K. Fey and H.-M. Kao, *J. Power Sources*, 2009, **189**, 256–262.
33 M. Gaberscek, R. Dominko and J. Jamnik, *J. Power Sources*, 2007, **174**, 944–948.
34 J.-M. Atebamba, J. Moskon, S. Pejovnik and M. Gaberscek, *J. Electrochem. Soc.*, 2010, **157**, A1218–A1228.
35 J. P. Schmidt, T. Chrobak, M. Ender, J. Illig, D. Klotz and E. Ivers-Tiffee, *J. Power Sources*, 2011, **196**, 5342–5348.
36 J. Illig, M. Ender, T. Chrobak, J. P. Schmidt, D. Klotz and E. Ivers-Tiffee, *J. Electrochem. Soc.*, 2012, **159**, A952–A960.
37 Y. Zhu, Y. Xu, Y. Liu, C. Luo and C. Wang, *Nanoscale*, 2013, **5**, 780–787.
38 R. Dominko, M. Bele, M. Gaberscek, M. Remskar, D. Hanzel, J. M. Goupil, S. Pejovnik and J. Jamnik, *J. Power Sources*, 2006, **153**, 274–280.
39 R. Dominko, M. Bele, M. Gaberscek, M. Remskar, D. Hanzel, S. Pejovnik and J. Jamnik, *J. Electrochem. Soc.*, 2005, **152**, A607–A610.
40 R. Dominko, J. M. Goupil, M. Bele, M. Gaberscek, M. Remskar, D. Hanzel and J. Jamnik, *J. Electrochem. Soc.*, 2005, **152**, A858–A863.
41 X. L. Wu, L. Y. Jiang, F. F. Cao, Y. G. Guo and L. J. Wan, *Adv. Mater.*, 2009, **21**, 2710–2714.

